ELSEVIER

Journal of Nuclear Materials 290–293 (2001) 250–254

journal of nuclear materials

www.elsevier.nl/locate/jnucmat

Characterisation of radiation and flux measurements on a neutraliser plate of the Tore Supra ergodic divertor

Y. Corre [a,*], R. Giannella [a], C. De Michelis [a], R. Guirlet [a], A. Azéroual [a], E. Chareyre [a], L. Costanzo [a], A. Escarguel [a], E. Gauthier [a], P. Ghendrih [a], J. Gunn [a], J. Hogan [b], P. Monier-Garbet [a], B. Pégourié [a], A. Pospieszczyk [c], E. Tsitrone [a]

[a] *Association Euratom-CEA sur la Fusion Contrôlée, CEA/Cadarache, F-13108 St-Paul-Lez-Durance, France*
[b] *Fusion Energy Division, Oak Ridge National Laboratory, Oak Ridge, TN 37830, USA*
[c] *Institut für Plasmaphysik, Forschungszentrum Jülich GmbH, Germany*

Abstract

A recent extensive experimental study of impurity production and penetration for various density regimes is described. Deuterium and carbon emissions near a neutraliser plate (NP) of the Tore Supra Ergodic Divertor (ED) has been measured with an absolutely calibrated visible endoscope, for high- and low-density plasma regimes. From these radiation measurements, we have deduced an effective carbon flux, and at an order-of-magnitude estimate of the NP erosion: 50 m for the fall 1999 experimental ED campaign (≈500 shots). Combining the measured carbon and deuterium fluxes, we deduce a global experimental carbon sputtering yield for the NP in the range 2×10^{-2}–3×10^{-1} for ohmic pulses, showing evidence of the importance of carbon self-sputtering.

Keywords: Carbon and deuterium radiation; Flux measurement; Sputtering

1. Introduction

The impurity screening effect and radiation efficiency at the plasma edge are intimately connected to impurity generation and transport. In order to understand and control these effects in Tore Supra Ergodic Divertor (ED) plasmas, it is necessary to study the behaviour of the impurity production and penetration for various density regimes [1]. A recent extensive experimental study of these phenomena is the object of this paper.

Radiation measurements and flux particle calculations, concerning the region in front of [2,3] and behind [4] the Outboard Pump Limiter (OPL), have been described in the past. This diagnostic has proven to be a useful tool to investigate the spatial localisation of radiation near a material structure [5]. An improved version of this diagnostic has been used to study the region in front of an equatorial plane ED target plate neutraliser [6].

The ED creates a small peripheral magnetic perturbation by means of six toroidally spaced octopolar field coils; as a result, the edge magnetic field configuration is ergodised, and the extracted ion flux is concentrated onto adapted B_4C neutraliser plates (NPs). Seven actively cooled NPs are poloidally arranged on each of these modules; most of the recycling ($D^+ \rightarrow D$, or $D^+ \rightarrow D_2$) and sputtering (physical, $D^+ \rightarrow C$, or chemical, $D^+ \rightarrow C_xD_y$) processes occur in this region. Although the NPs are originally B_4C coated, TS is an all-carbon device, and redeposited carbon quickly covers all the internal plasma facing components (no boron is spectroscopically seen, already a few shots after boronisation). As a consequence, the main plasma–surface interaction processes concern only carbon. The present data are taken from two experimental scenarios with a

* Corresponding author. Tel.: +33-44 56 375; fax: +33-44 22 54 990.
E-mail address: corre@drfc.cad.cea.fr (Y. Corre).

0022-3115/01/$ - see front matter
PII: S0022-3115(00)00625-5

density ramp ($n_e^{edge} = 0.2–1 \times 10^{19}$ m^{-3}; $T_e^{edge} = 60–10$ eV).

2. Experimental setup

The main diagnostic used in this study is a visible endoscope, located in a top part of the torus, enabling views of the internal components of the machine (OPL, antennae, or one of the equatorial plane NPs). Light is guided to the endoscope imaging system by a movable mirror (inside the vacuum vessel), and an optical sleeve consisting of a sapphire window and relay lenses. Outside the vacuum vessel, light is divided by a beam splitter for simultaneous measurements by a CCD camera (high spatial resolution, 1 mm/pixel, low spectral and temporal resolution, 100 ms), and by a set of optical fibres connected to a visible spectrometer (low spatial resolution, high spectral and temporal resolution). The CCD camera is equipped with interchangeable interference filters, allowing to measure (on a shot-to-shot basis) the Dα (6561 Å) and CII (5145 Å) spectral lines. The other path from the beam splitter leads to three optical fibres, providing spectral resolution for selected zones of the endoscope field of view. These fibres have been used to determine the absolute calibration of the CCD images at the wavelengths of interest. The total (systematic and statistical) uncertainty of the brightness measurement is estimated at 30%.

3. Radiation in the region near the NP

3.1. Localisation of the radiation

Although the NP region interacting with the plasma is approximately plane, it is necessary to look at the influence of its geometry on the radiating map. The NP is made of four identical fingers, separated by three vents, designed for particle collection (Fig. 1). These vents are terminated by V-shaped notches (also named V-point, to which the field lines are connected with an incidence angle close to normal); consequently, the incident flux is higher here than on any other region. Another region of intense plasma–surface interaction is the Langmuir probe located in the central vent; indeed, the domed probe [7] penetrates slightly more into the plasma than the surrounding surface, resulting in peaked recycling and sputtering in this region. A CCD image of the NP (Dα wavelength), on which we have superimposed its geometry and the six different chords used for the data in this paper (along the fingers, L_1, L_2, L_3, and perpendicular to them, l_1, l_2, l_3), is shown in Fig. 1. No chord along the fourth finger has been taken, since the magnetic shadow of the nearby OPL (~2.5 m upstream) is cast upon this region.

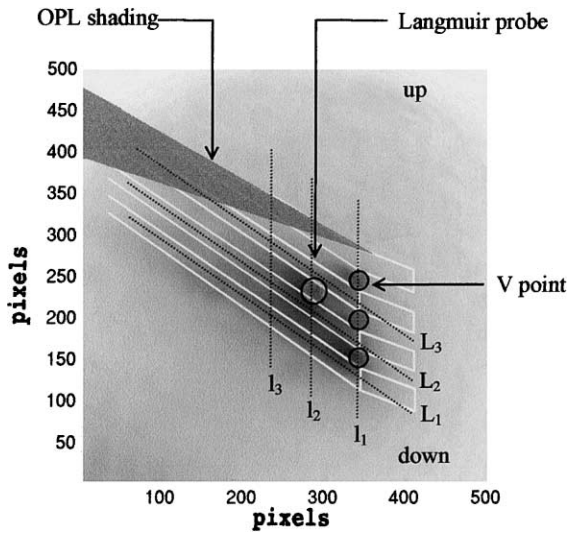

Fig. 1. CCD picture (Dα wavelength) with superimposed neutraliser plate geometry (white lines represent the edges of the fingers) and chords along which the profiles discussed below have been taken (dotted lines).

Fig. 2 shows the Dα brightness profiles along the six chosen chords. The upper part (chords across the fingers; the two dotted vertical lines delimit the neutraliser region from the CFC tile structure of the ED modules) shows that the average brightness from the NP is considerably larger than that from the surrounding structure (above the CFC tiles). The l_1 profile has three radiation peaks due to the V-point structure in each vent (light grey shadowed regions in the figure); as expected, the Dα radiation enhancement on the lower V-point is the largest one, since it is not affected by the probe (contrary to the middle V-point) or LPM (contrary to the upper V-point) shadows, and comes from a relatively small surface of roughly 1 cm^2. This enhancement, as well as the relevant surface, is smaller for the CII radiation. The radiation increase on the l_2 profile clearly shows the effect of the Langmuir probe coming from a larger surface (with a linear dimension of approximately 4 cm). Finally, on the l_3 profile, which is farther away from the NP notches, the V-point and probe effects are strongly attenuated.

The lower part of Fig. 2 shows the longitudinal profiles parallel to the finger structure; the radiation profile intensities increase approximately linearly along the fingers, up to a maximum just before their upper part (indicated by the full line). Only the middle chord, L_2, is affected by local phenomena; the effect of the Langmuir probe is clearly seen. The linear decrease occurs on a distance of approximately 17 cm, which can probably characterise the extent of the 'wetted zone' of maximum incident flux. From these data, we can experimentally estimate the wetted surface of the NP from the radiative behaviour of Dα : $S_{wet} = 17 \times 10$ cm^2.

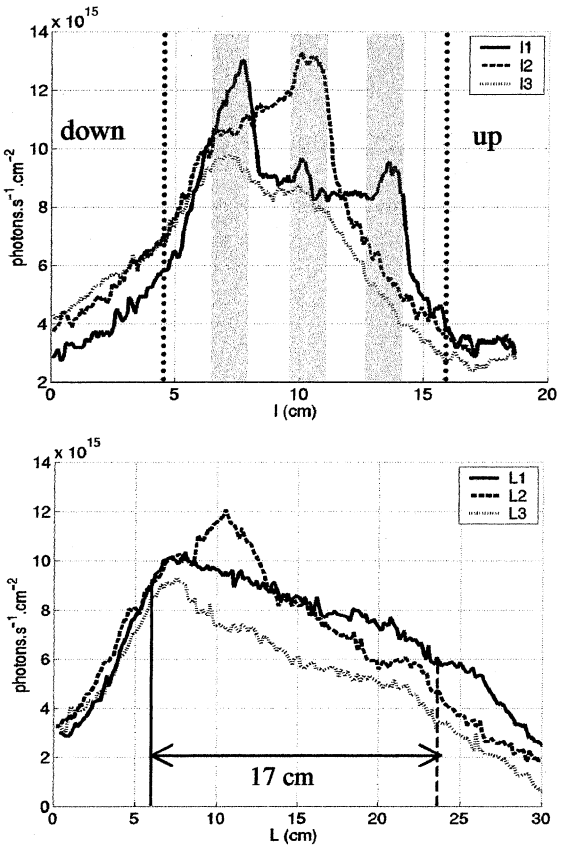

Fig. 2. Dα brightness profiles along the three transversal chords (top), and along the three lower fingers (bottom).

3.2. Evolution of the radiation with the electron density

The ED configuration is characterised by the existence of three density regimes: (1) the linear regime at low plasma density, with $n_e^{edge} \propto \langle n_e \rangle$; (2) the high recycling regime, with $n_e^{edge} \propto \langle n_e \rangle^3$; and (3) the semi-detached regime, with n_e^{edge} decreasing with increasing $\langle n_e \rangle$. Two equivalent ohmic pulses with a density ramp have been selected in the low recycling regime (#27627, 27632), and two in the high recycling regime (#27633, 27644). Fig. 3 compares the radiative CII profiles (along chords l_1 and L_1, normalised to their peak value), at low and high density ($n_e^{edge} = 0.2 \times 10^{19}$ and 1×10^{19} m^{-3}). Together with the corresponding Dα pictures, the data show that the Dα and CII brightnesses increase with the electron density; their profiles remain essentially unchanged in shape over the entire density range. Note that the Dα and CII radiations remain attached to the neutraliser structure, with no profile spread or elongation as the density increases (the semi-detached regime is not considered in this paper).

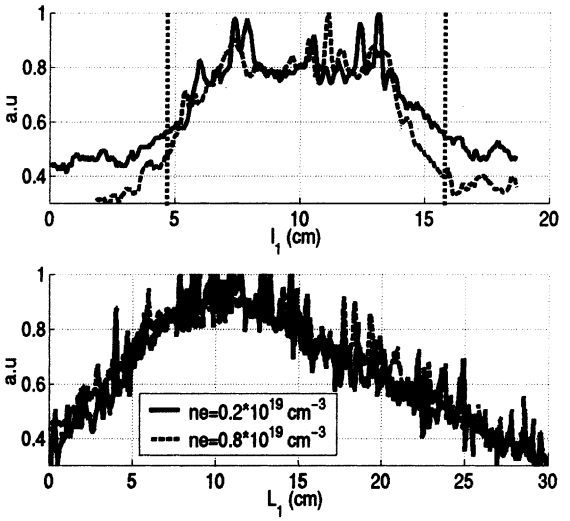

Fig. 3. Normalised CII brightness profiles along the transversal chord over the V-points (top), and along the lower finger (bottom), at two different edge electron densities.

4. Flux and sputtering yield estimations

4.1. Flux calculation

The next step in the data analysis is to calculate the D^0 and C^{1+} influxes using the endoscope images, on which it is easy to select a region non-polluted by local effects, such as shadowing, probe, or V-point. Our work area is a rectangle of approximately 2 cm^2, located under the Langmuir probe on the lowest finger (see Fig. 1). The influxes are estimated, using the standard equation [8], from the absolute brightnesses in the selected region. Input data for this estimation are the local n_e and T_e values (measured by the Langmuir probe installed in the middle NP vent [7]), needed to calculate the number of ionisations per photon of the relevant transitions (using the atomic physics database ADAS [9]).

Assuming that the wall is saturated by deuterium, we shall first estimate the global deuterium balance between the incident ions coming from the plasma and the emitted neutrals resulting from the recycling process. Fig. 4 compares the incident D^+ flux (Φ^{out}) measured by the Langmuir probe, and the neutral deuterium flux (Φ^{in}) measured via the Dα radiation, by the endoscope system, for two ohmic pulses, at low (#27632) and high density (#27644), respectively. A reasonable agreement between the two fluxes is found (especially as far as the temporal trend is concerned); the factor of two difference in the low-density case (TS27632, up to 6 s) may be due to the large Z_{eff} value of this plasma [10], possibly resulting in a significant carbon contamination of the incident flux detected by the probe. Moreover, a recent comparison between the Dα endoscope measurements

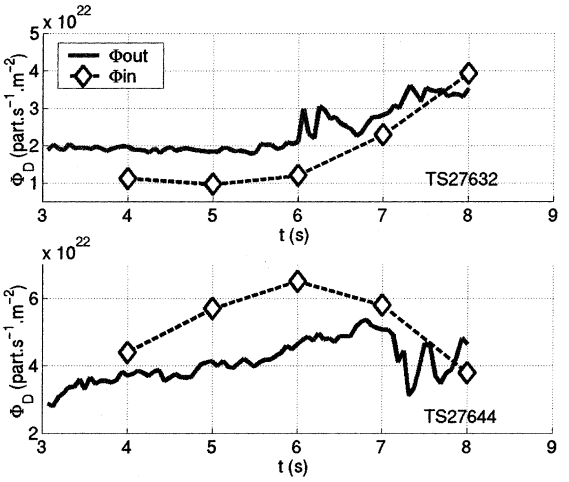

Fig. 4. D^0 influx measured with endoscope (Φ_{in}) and incident D^+ flux measured by the Langmuir probe (Φ_{out}) for two density ramp up pulses (TS27632 at low density and TS27644 at high density).

and the results of a simulation using the code ED-COLL has also shown a satisfactory agreement [11].

The deuterium and C^{1+} influxes, measured by the endoscope system, are plotted as functions of the edge electron temperature in Fig. 5. The emitted D^0 flux exhibits the same dependence on n_e and T_e as the incident D^+ flux ($\Phi_{inc} \propto n_e^{edge}\sqrt{T_e^{edge}}$) down to $T_e \approx 15$ eV. Below this value, the flux decrease indicates the transition to the semi-detached regime. On the other hand, the carbon influx decreases continuously with decreasing edge electron temperature. This is expected at low temperatures (high recycling regime, ☆ points on the figure), since the decrease of the physical sputtering yield, for $T_e < 30$ eV, is steeper than the incident flux increase (in this temperature range the sputtering yield varies as $Y_{phys} \propto T_e^3$ [12]). In the same figure, we compare the predicted influx of neutral carbon, calculated by BBQ (a plasma–surface interaction 3D Monte Carlo code [13], recently adapted to the ED configuration [14]), including only physical sputtering, with the experimental influx measurements. The difference at higher temperatures (◇ points) is possibly due to self-sputtering processes ($C^{n+} \rightarrow C^0$) becoming more important with increasing edge temperature (see below). Although the incident carbon flux is smaller than the deuterium incident flux, self-sputtering can play an important role for carbon generation at the largest values of the edge temperature; in this range, the Z_{eff} value is quite large [10]. Note that it was not possible to have images of the NP in the neutral carbon light (9080 Å interference filter), mainly because of the low sensitivity of the CCD camera at this wavelength. However, since the neutral carbon ionisation rate is very large for our plasma parameters, we have assumed that the C^{1+} flux represents the carbon source (this has been validated a posteriori by the BBQ code). Finally, the carbon flux from the NP is in the range:

$$7 \times 10^{20} < \Phi_C^{in} < 6 \times 10^{21} \text{ particle s}^{-1} \text{ m}^{-2} \quad (1)$$

for $10 < T_e^{edge} < 60$ eV. It must, moreover, be noted that the BBQ simulations indicate that carbon redeposition can not be neglected, especially in the high recycling regime.

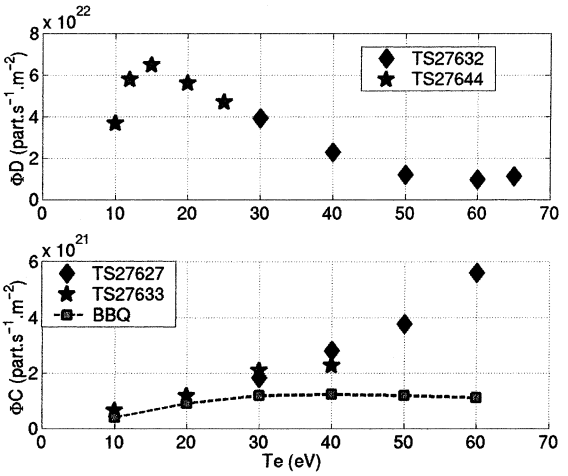

Fig. 5. Experimental and simulated carbon fluxes (bottom) and experimental deuterium flux (top) as a function of the edge electron temperature.

4.2. Erosion measurements

Neglecting carbon redeposition, we can estimate the NP eroded thickness over the entire fall 1999 campaign. Considering only ohmic shots ($N_{shot} = 517$) and an average carbon flux from the endoscope measurement ($\langle\Phi_C\rangle = 2.5 \times 10^{21}$ particle s^{-1} m^{-2}), we obtain a gross erosion of approximately 50 μm. This must be compared with the 10 μm directly measured by the ultrasonic probe after the end of the experimental campaign [15] (which, however, included also a relatively small number of shots with moderate additional power). Given the approximations involved in our evaluation, and the fact that we have neglected redeposition, this order of magnitude agreement can be considered as satisfactory.

4.3. Sputtering yield estimation

The ratio of the C^{1+} flux (equivalent to the carbon source) to the D_0 flux (equivalent to the incident D^+ flux) gives an estimation of the total carbon sputtering yield; this is plotted in Fig. 6 as a function of the edge electron temperature. This figure also shows the theoretical physical sputtering yield [12] Y_{ps} adapted to the

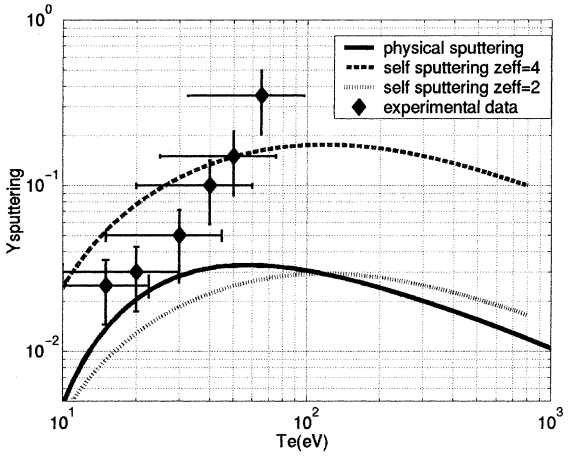

Fig. 6. Experimental carbon sputtering yield and theoretical data for physical and self-sputtering contribution for $Z_{\text{eff}} = 4$ and $Z_{\text{eff}} = 2$, as a function of the edge electron temperature.

T_e^{edge} abscissa using the sheath theory [16]. Note, however, that the theoretical sputtering yields assume an incoming ion flux at normal incidence; in the experiments, the average incident angle of field lines on the NP is in the range $12° > \alpha > 6°$. The experimental curve is clearly higher than Y_{ps} for T_e^{edge} above 20 eV and has a different dependence on this parameter. Fig. 6 shows heuristic estimates of the self-sputtering contribution for $Z_{\text{eff}} = 4$ (as measured above $T_e^{\text{edge}} = 50$ eV), and $Z_{\text{eff}} = 2$ (a typical value for lower temperature). It appears that self-sputtering can quantitatively account for the difference observed between the evaluated sputtering yield and Y_{ps}.

5. Conclusion

This paper describes an extensive study of radiation from the equatorial NP of one of the ED modules. The endoscope data show that the radiation of deuterium neutrals and of the carbon impurity source is localised on the NP. From the endoscope images, we have evaluated the deuterium and carbon fluxes from the NP. In spite of the assumptions inherent to these evaluations, the estimated D_0 flux is in reasonable agreement with the D^+ incident flux measured by the Langmuir probe. The estimated carbon flux strongly increases for edge electron temperature values above a few tens of eV, which seems to point out to C self-sputtering as an important C production mechanism. These data confirm that the high recycling regime is favourable from the point of view of impurity generation, as seen when studying the dependence on T_e^{edge} of Z_{eff} and of the carbon concentration in the confined plasma [10]. Finally, we have evaluated, assuming that no redeposition occurs, the gross carbon erosion during the fall 1999 campaign; although the estimated value of 50 μm is five times larger than the net value measured in a post-mortem analysis of the NP, the evaluation presented here seems to give the right order of magnitude for the thickness of the eroded layer.

References

[1] P. Ghendrih et al., Plasma Phys. Control. Fus. 39 (1997) B297–B322.
[2] S.J. Tobin et al., Plasma Phys. Control. Fus. 38 (1996) 251–263.
[3] S.J. Tobin et al., Plasma Phys. Control. Fus. 40 (1998) 1335–1348.
[4] R. Ruggiéri et al., J. Nucl. Mater 266–269 (1999) 660–665.
[5] F. Meo, Thesis. Université du Québec, INRS-Energie et Matériaux, 1999.
[6] L. Chérigier et al., in: Proceedings of the 24th EPS Conference On Controlled Fusion and Plasma Physics, Vol. 21, Berchtesgaden, 1997, p. 201.
[7] J.P. Gunn et al., Plasma Phys. Control. Fus. 41 (1999) B243–B257.
[8] K. Behringer et al., Plasma Phys. Control. Fus. 31 (1999) 2059–2099.
[9] H.P. Summers, Atomic Data Analysis Structure, JET Report IR (94) 06.
[10] P. Monier-Garbet et al., this Conference.
[11] A. Azeroual et al., Nucl. Fus. (to be published).
[12] J. Roth, C. Garcia-Rosales, Nucl. Fus. 36 (1996) 1647 (with corrigendum Nucl. Fus., 1997, p. 897)
[13] J. Hogan et al., in: Proceedings of the 16th IAEA Conference On Controlled Nuclear Fusion, Montreal, 1996, Vienna, 1997, Vol. 2, p. 625.
[14] R. Giannella et al., Plasma Phys. Control. Fus. (to be submitted).
[15] E. Tsitrone et al., this Conference.
[16] P.C. Stangeby, G.M. McCracken, Nucl. Fus. 30 (7) (1990).